-------------------------------------------------------------------------------------------------------

# STUDY ON EARTHQUAKE DAMAGE MECHANISM OF AQUEDUCT STRUCTURE BASED ON DIFFERENT BOUNDARY

*Xinyong Xu[1, 2], Xuhui Liu[1], Cheng Zhang[3], Xinyun Xu[4], Jianwei Zhang[1, 2]*

1. *School of Water Conservancy, North China University of Water Resources and Electric Power, Zhengzhou 450046, China; xuxinyong@ncwu.edu.cn*
2. *Collaborative Innovation Center of Water ResourcesEfficient Utilization and Protection Engineering,Henan Province; Zhengzhou 450046, China*
3. *Changjiang River Scientific Research Institute of Changjiang Water Resources Commission, Wuhan 430000, China; 277523266@qq.com*
4. *China Three Gorges Pearl River Power Generation Co., Ltd.,Guangzhou 510000, China; 854014625@qq.com*

## ABSTRACT

Numerically simulating an infinite domain foundation is an important method for solving structural dynamics problems. This paper introduces several artificial dynamic boundaries commonly used in the study of structural dynamics, and elaborates the theory and methods of the dynamic infinite element method boundary (IEMB) and viscous–spring artificial boundary (VSAB). The capacity of different boundary effects on seismic waves energy absorption is verified by establishing a layered half-space model. An irrigation aqueduct is taken as a research object. The IEMB, VSAB, and fixed boundary (FB) models are established and the Concrete Damaged Plasticity (CDP) constitutive is introduced, which is aimed at studying the dynamic failure mechanism and the rules of damage development to the aqueduct structure during the seismic duration. The results for the IEMB and VSAB show better energy absorption for the incident waves and a better simulation result for the damping effect of the far field foundation than that of the FB. Comparing the maximum displacement response rules of the three boundaries, it is seen that the maximum displacement response values of the VSAB and dynamic IEMB increased by 6%–48% and 9%–35%, respectively, over the FB. The calculation results of the VSAB are similar to that of the IEMB. The difference between the maximum acceleration response values is 2%–17% whereas the difference between the maximum displacement response values is 0.4%–19%. The IEMB studied in this paper provides a theoretical reference for large–scale building boundary treatment in structural dynamics calculations.

## KEYWORDS

Irrigation aqueduct, Viscous–spring boundary, FEM–IEM interaction, Concrete damage plasticity, Seismic damage

## INTRODUCTION

Aqueducts are a commonly used cross water transmission facility in water conservancy projects, and have the functions of irrigation, water delivery, and water supply. Numerous agricultural irrigation areas are located in earthquake–prone areas. Due to the high functional requirements for safe water transport, a study of the failure mechanism of the aqueduct structure under seismic loading can ensure the safe operation of aqueducts and the normal dispatching of water resources in irrigated areas.

To date, many achievements have been made in studying the mechanical properties of

-------------------------------------------------------------------------------------------------------

aqueducts. Following the existing theory regarding small amplitude water sloshing, fluid–structure interaction between water and structure is usually considered in the previous dynamic analysis of water tanks [1–3]. The water tank and aqueduct are similar in structures, so some scholars considered the effect of fluid–structure interaction examined the dynamic failure mechanism of the aqueduct structures under earthquake ground motion [4–7]. Li, et al. [8] studied the seismic ground motion response to the long span of large–scale aqueduct structures by a simplified beam–water coupled system. Besides, some researchers have used different theoretical methods to study the seismic analysis of aqueduct structures under the influence of earthquakes [9, 10]. It can be seen from the above studies that numerical simulation is still a powerful tool to solve such problems in seismic engineering and aqueduct structural analysis. However, the propagation of seismic wave motion energy in the foundation and the reflection effects at the boundary conditions play a significant role in determining whether the dynamic calculations can achieve reasonable results.

The finite domain simulation of the seismic waves motion propagation used in traditional finite element calculations is prone to reflection on artificial boundaries and propagation of interference waves. Lysmer and Kuhlemeyer [11] first proposed a viscous boundary with a simple form but this was not suitable for the multidimensional situations of complex structures. Deeks and Randolph [12] considered soil–structure interaction (SSI) problems under dynamic action and proposed the earliest viscous–spring boundary based on the viscous boundary, and the numerical simulation example of transient radiation model problems was used to solve the transient SSI problems in the time domain. Gu, et al. [13] derived the viscous-spring artificial boundary (VSAB) equation based on the wave motion equation, demonstrated the high precision and adequate stability of a three–dimensional (3D) VSAB through a calculated example, and presented the concept of a consistent VSAB. Liao and Wong [14] presented and improved the transmitting boundary formula, and used multiple transmission methods to simulate the physical process of wave motion propagation. This method moderately improved the accuracy but the implementation process was more complicated. The infinite element method boundary (IEMB) is a numerical method based on the infinite element theory and developed to solve the infinite domain problem. In 1973, Ungless [15] first proposed the infinite element theory. Bettess [16] proposed mapping infinite elements for the first time based on the mapping between global coordinates and local coordinates, which is called Bettess elements. Zienkiewicz, et al. [17] based on the improvement of the work of Bettess elements, proposed the definition of mapping infinite elements and applied it to solve exterior wave problems. Yun, et al. [18] proposed and studied a new infinite element method to solve the two–dimensional (2D) and 3D pier-soil dynamic interaction in the frequency and time domains. The study results were verified by the applicability of dynamic IEMB, which has a better filtering effect on scattered waves than the VSAB [19]. Infinite element can be combined with finite element. The finite element method is used to simulate the near-field region, while the infinite element method is used to simulate the far-field region. The experience of many scholars in solving infinite domain problems shows that [20-23]: the coupling model of finite element and infinite element has extensive practicability in solving practical engineering problems, and that shows obvious advantages in simulating and approximate simulating infinite domain problems. In a word, it is often used to solve more complex unbounded problems together with the conventional finite element method, which is a supplement to the finite element method. Therefore, it has inherent coordination with the finite element method and has more advantages than other numerical methods such as viscous boundary method for solving unbounded domain problems. But, Dynamic IEMB has not been widely used in engineering as a method to solve 3D multidirectional mapping problems.

Based on the above factors, FB, VSAB and IEMB are used to simulate the infinite domain foundation to reflect the energy dispersion phenomenon of incident waves at different boundaries. The CDP constitutive [24–26] is introduced in this paper, which is aimed at studying the dynamic failure mechanism and the rules of damage development for concrete aqueduct structures subject to seismic ground motion.

---------------------------------------------------------------------------------------------------------

# DYNAMIC INFINITE ELEMENT BOUNDARY (IEMB) METHOD

## IEMB principle

In the solution of dynamic problems, the model boundary may produce a boundary effect, in which the energy reflected on the computing domains and affects the calculation results. The IEMB of ABAQUS provides the first– and second–order infinite elements, the finite–infinite element method (FEM–IEM) interaction is used to simulate the infinite domain propagation of the far–field seismic waves motion. By defining an element with a decay function in the semi–infinite domain, the FEM–IEM interaction method is realized, which overcomes the defects of the finite element method.

The dynamic response to IEMB is considered based on a traveling plane wave with orthogonal boundaries. Therefore, it is assumed that the response adjacent to the boundary has a sufficiently small amplitude that deforms the medium in a linear elastic manner. Its equilibrium equation can be described as follows:

$$-\rho \ddot{u} + \frac{\partial}{\partial x} \cdot \sigma = 0 \tag{1}$$

where $\rho$ is the mass density of the medium, $Kg \cdot m^{-3}$; $\ddot{u}$ is the acceleration of the material particles, $m \cdot s^{2}$; $\sigma$ is the stress, $Pa$; and $x$ is the position. The material is assumed to be isotropic and linearly elastic; therefore, $\sigma$ can be described by

$$\sigma = \lambda \prod : \varepsilon + 2G\varepsilon \tag{2}$$

where $\lambda$ and $G$ are functions expressing lame constants and the shear modulus of the medium, respectively; $\lambda = Ev / (1+v)(1-2v)$, $G = E / 2(1+v)$ ( $E$ is Young's modulus, $v$ is Poisson's ratio), and $\varepsilon$ is the strain.

When the material response is introduced into the equations of equilibrium, and $\varepsilon$ is assumed to be a small strain, $\varepsilon$ is can be computed by the following equation:

$$\varepsilon = \frac{1}{2}\left\{ \frac{\partial u}{\partial x} + \left[ \frac{\partial u}{\partial x} \right]^{\mathrm{T}} \right\} \tag{3}$$

Substituting Equations (2) and (3) into Equation (1), the governing equation of motion is obtained.

$$\rho u_i = G \frac{\partial^2 u_i}{\partial x_j \partial x_j} + (\lambda + G) \frac{\partial^2 u_j}{\partial x_i \partial x_j} \tag{4}$$

Assuming that the plane wave is along the $X$–axis, the equation has the following two forms of solution. Equation (5) describes the plane $P$–wave (longitudinal wave), and Equations (6) and (7) express the plane $S$–wave (shear wave).

$$u_x = f(x \pm c_{\mathrm{p}}t), \ u_y = u_z = 0 \tag{5}$$

$$u_y = f(x \pm c_{\mathrm{s}}t), \ u_x = u_z = 0 \tag{6}$$

$$u_z = f(x \pm c_{\mathrm{s}}t), \ u_x = u_y = 0 \tag{7}$$

where $c_p = \sqrt{\dfrac{\lambda + 2G}{\rho}}$ and $c_s = \sqrt{\dfrac{G}{\rho}}$, "-" indicates forward propagation along $X$, "+" indicates backward propagation along $X$.

To avoid the reflection of the $P$–wave and $S$–wave energy back to the finite domain medium of $X < L$, damping constants $d_p$ and $d_s$ are introduced to calculate distributed damping at the boundary junction of the finite domain and infinite domain ( $X = L$ ). The damping stress can be

expressed as:

$$\sigma_{xx} = ma - d_p \dot{u}_x \tag{8}$$

$$\sigma_{xy} = -d_s \dot{u}_y \tag{9}$$

$$\sigma_{xz} = -d_s \dot{u}_z \tag{10}$$

in which $\sigma_{xx}$ is the P–wave stress at the boundary junction of the finite domain and infinite domain. $\sigma_{xx} = (\lambda + 2G)(f_1' + f_2')$, the other stress component $\sigma_{ij} = 0$, and the velocity is $\dot{u}_x = -c_p(f_1' - f_2')$. Equation (11) can be obtained using the above equations.

$$(\lambda + 2G - d_p c_p)f_1' + (\lambda + 2G + d_p c_p)f_2' = 0 \tag{11}$$

To ensure that there is no reflected stress wave at the boundary position when the wave is incident in any form, it is necessary to ensure $f_2 = 0$ and $f_2' = 0$. The P–wave damping form can be deduced as follows:

$$d_p = \frac{\lambda + 2G}{c_p} = \rho c_p \tag{12}$$

As in the previous sections, the damping form of the S–wave can be determined as follows:

$$d_s = \rho c_s \tag{13}$$

It should be noted that the IEM method is the boundary treatment method for FEM–IEM interaction. By introducing these boundary damping values to avoid waves reflection effects at the location of a boundary, we can adequately simulate the propagation of wave motion in the infinite domain.


**Viscous-spring artificial boundary (VSAB) method**

Because the VSAB has been widely used in engineering, it is not derived in detail here. The specific derivation process can be found in [27]. Its implementation method in ABAQUS can be seen in Figure 1.
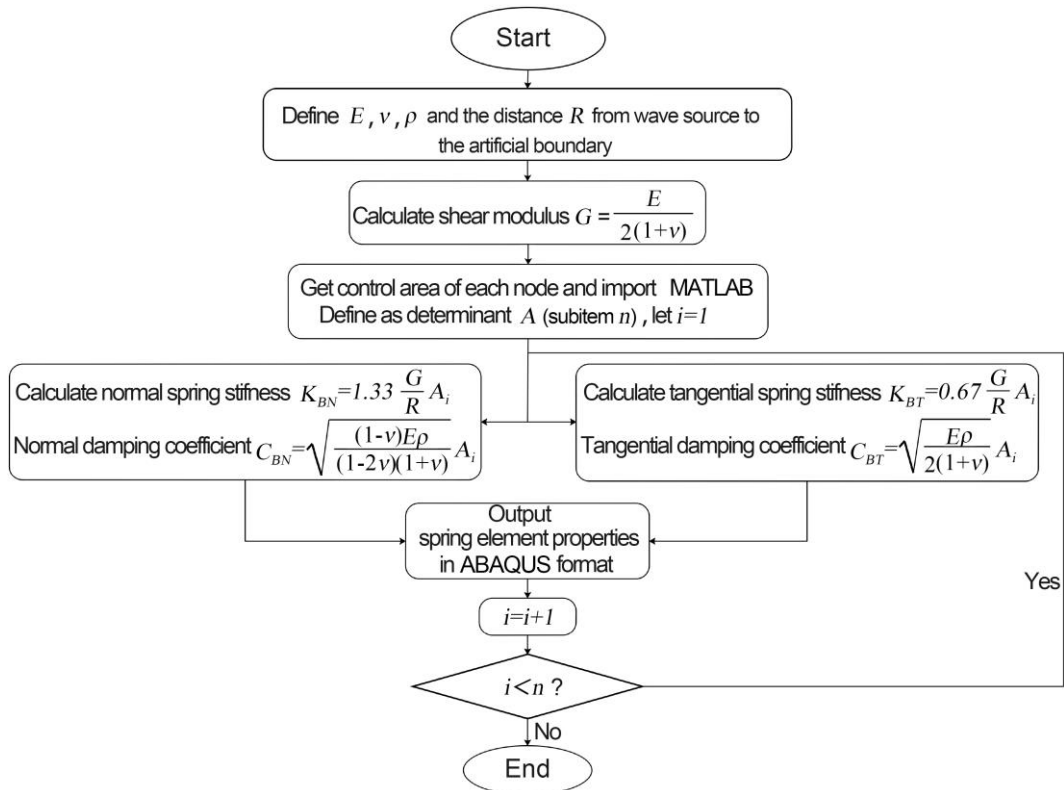
-------------------------------------------------------------------------------------------------------



*Fig. 1 – Flow chart of viscous–spring artificial boundary realization*

## Examples of numerical simulations

To verify the accuracy and reliability of the IEMB calculation method in the seismic responses of the aqueduct, the model of a 3D elastic homogeneous half–space was established by using the ABAQUS FEM code, considering the Lamb problem [28].

In this example, non-dimensional units are used. The range of the numerically computed object is taken as: $-0.5 \leq x, y \leq 0.5$ , $-0.5 \leq z \leq 0$ with the finite element size taken as $\Delta x = \Delta y = \Delta z = 0.05$ . Young's modulus of the medium $E = 40$, Poisson's ratio $v = 0.25$, and mass density $\rho = 1$. The duration $T = 5.0s$ and time interval $\Delta t = 0.001s$ are used for this example.
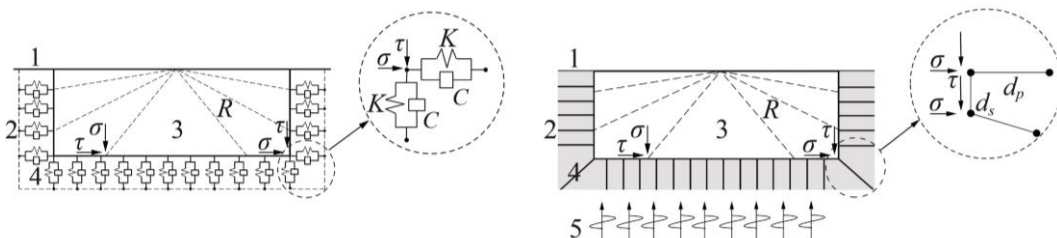


*(a) Viscous-spring artificial boundary; (b) Infinite element method artificial boundary*
*Fig. 2 – Schematic diagrams of viscous–spring and infinite element method artificial boundary*

*Note: *1.Free surface; 2. Infinite domain; 3. Near field; 4. Artificial boundary; 5. Seismic wave*
*$\sigma$ is the normal stress; $\tau$ is the shear stress; $K$ is the spring stiffness; $C$ is the damping coefficient; $d_p$ is the normal damping; $d_s$ is the tangential damping; $R$ is the distance between the observation point on the free surface and the vertical load point.*

-----------------------------------------------------------------------------------------------------

Ignoring the dissipation effect of waves in the medium, the VSAB, IEMB and FB are respectively set at the boundary truncation position and compared with the analytical solution in this example. The VSAB and IEMB are shown in Figure 2. The time history of applying the load is shown in Figure 3(a), which acts on the free surface of the semi–infinite space as a concentrated vertical force. The observation points 0.2 and 0.4 away from the loading center point $O$ are selected and analysed by calculating the relative displacement. The schematic diagram of the observation point is shown in Figure 3(b).
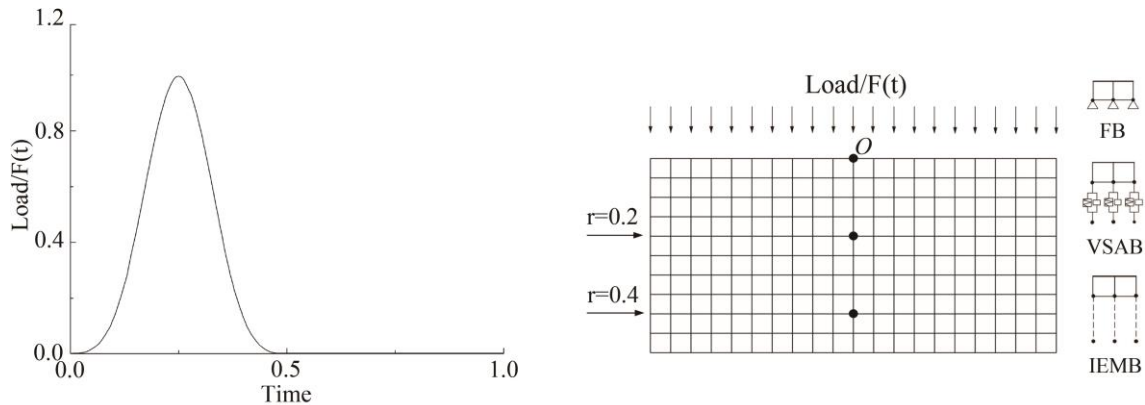


*(a) Load time history; (b) Observation points of different boundary finite element model*
*Fig. 3 – Finite element model and load time history curve*

The relative displacement time histories in the vertical direction for each observation point under different boundary effects are shown in Figure 4. The analytical solution can be obtained by the integration of the fundamental solution for the load time histories. It can be seen from Figure 4 that the FB cannot cause nodes movement when the load is applied from the top of the model to the bottom. That is, the nodes at the bottom of the calculation model do not move in the FB condition, and the wave is reflected back to the elastic medium. Since there is no damping effect in the medium, the displacement curve oscillates back and forth in the medium elastic region, forming the displacement curve in Figure 4. When the VSAB is adopted, as shown in Figure 4, most of the energy is absorbed on the VSAB, while a small part is reflected back to the medium elastic area, and also absorbed in the following time period. However, when the IEMB is adopted, there is no energy reflection on the FEM–IEM interaction boundary. Results show that under the FB condition, the wave motion is almost entirely reflected. In contrast, the VSAB and IEMB show good energy absorption effect, and the wave propagation is almost completely dissipated on the boundary.
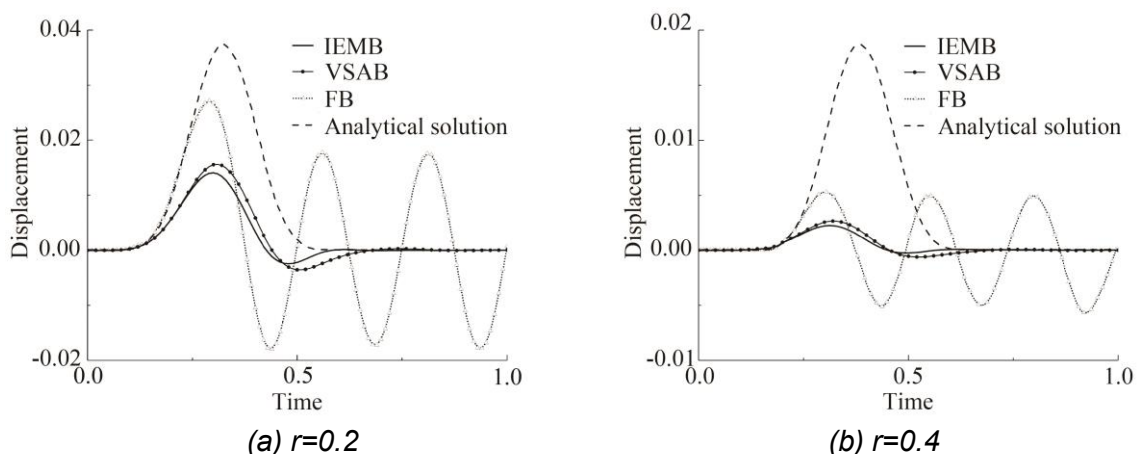


*(a) r=0.2*　　　　　　　　*(b) r=0.4*
*Fig. 4 – Contrast diagram of the effect of each characteristic point on three boundary*

-----------------------------------------------------------------------------------------------------------------

# SEISMIC GROUND MOTION FAILURE MECHANISM OF AQUEDUCT STRUCTURE BASED ON IEMB

The above analysis shows that the VSAB and IEMB have a good absorption effect on seismic waves compared with the FB, which can better simulate the procedure of wave motion propagation. However, it is not easy to evaluate how much influences this simulation has on the calculation of the actual project. The following is an example of a large–scale aqueduct actual project in a Chinese irrigation district, and the effects of the three boundaries are compared.

## Example model and seismic wave selection

A three–span structure of the aqueduct is selected for this study. The overall structure includes the groove body, bent, bent column, and foundation, etc. The groove body is a rectangular structure with a single span length of 10 m. Figure 5 shows the bent which has an h–form frame structure, the aqueduct is 1.8 m wide and 2 m high, and the bent is 7.6 m high. C30 concrete is used to construct the groove body, and the CDP constitutive structure is introduced to simulate the dynamic damage development of concrete [24–26].
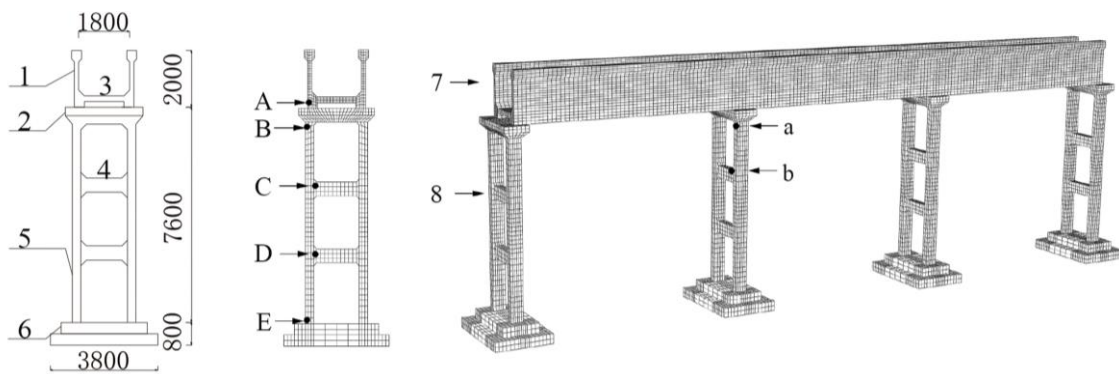


(a) Aqueduct structure diagram;     (b) Finite Element Model of Aqueduct Structure
Fig. 5 – Aqueduct Structure Diagram and Finite Element Model

Note: *1. Wing wall; 2. Pier cap; 3. Bottom plate; 4. Crossbeam; 5. Bent column; 6. Foundation platform; 7. Groove body; 8. Bent
A、B、C、D、E are feature points of damage; a、b are feature points of aqueduct structural seismic ground motion response.

The damage values range from 0 (no damage) to 1 (complete damage) to express the degree of damage to different materials. The various material parameters of the aqueduct structure are shown in Table 1.

Tab. 1 - Various material parameters of aqueduct structure

| Material | Elastic modulus/(GPa) | Density /(Kg·m$^{-3}$) | Poisson ratio | Tensile strength/(MPa) | Compressive strength/(MPa) |
|---|---|---|---|---|---|
| Aqueduct(C30) | 30 | 2500 | 0.167 | 1.3 | 14.3 |
| Bent(C25) | 28 | 2450 | 0.167 | 1.27 | 11.9 |
| Foundation(C25) | 28 | 2450 | 0.167 | 1.27 | 11.9 |
| Ground | 7 | 2100 | 0.3 | – | – |

-------------------------------------------------------------------------------------------------------------

The numerical model based on the IEMB is shown in Figure 6. In dynamic analysis, the amplitude attenuation of the response wave depends on the damping effect of the structure. However, it is challenging to determine the damping matrix of the structure. Since the structure of the natural modes, the mass matrix $M$ is orthogonal to the stiffness matrix $K$, the damping matrix $C$ of the structure is usually simplified as a linear combination of $M$ and $K$.

$$C = \alpha M + \beta K \tag{14}$$

Rayleigh damping is used to analyse the equation. $\alpha$ and $\beta$ can be expressed in terms of Equations (15) and (16).

$$\alpha = \frac{2\omega_i\omega_j(\xi_j\omega_i - \xi_i\omega_j)}{\omega_i^2 - \omega_j^2} \tag{15}$$

$$\beta = \frac{2(\xi_j\omega_j - \xi_i\omega_i)}{\omega_j^2 - \omega_i^2} \tag{16}$$

where $\omega_i$ and $\omega_j$, respectively, take the first and second–order frequencies corresponding to the structure, and $\xi_i$ resp. $\xi_j$ take the damping ratio corresponding to the structure frequency.

The engineering foundation site classification is Class I, and the basic seismic intensity is VIII. The horizontal peak acceleration of rare ground motion is 0.331g, and the vertical peak acceleration is taken as two–thirds that of the horizontal direction. Following the principle of similar spectrum characteristics, the artificial wave TH3TG025 was selected as the seismic wave. The duration was set using 10% of the peak acceleration as the threshold [29]. The duration is calculated as 5 s, which meets the standard requirements of 5–10 times the basic period of the structure, time interval $\Delta t = 0.02 s$, and the acceleration time history of the seismic wave is shown in Figure 7.
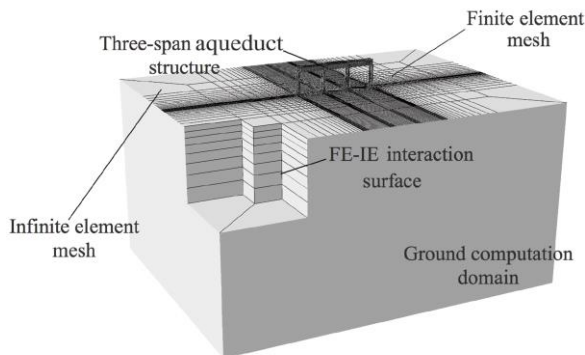


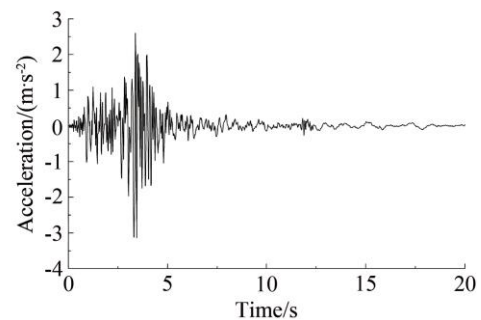Fig. 6 – FE–IE interaction foundation model



Fig. 7 – Time history records of seismic accelerations

## Seismic ground motion response rules for the structure

### *Aqueduct structure acceleration response rules*

The numerical calculation selects the top a of the bent and crossbeam end b as feature points for the seismic ground motion response analysis of the aqueduct. The results are presented in Figure 8.

--------------------------------------------------------------------------------------------------
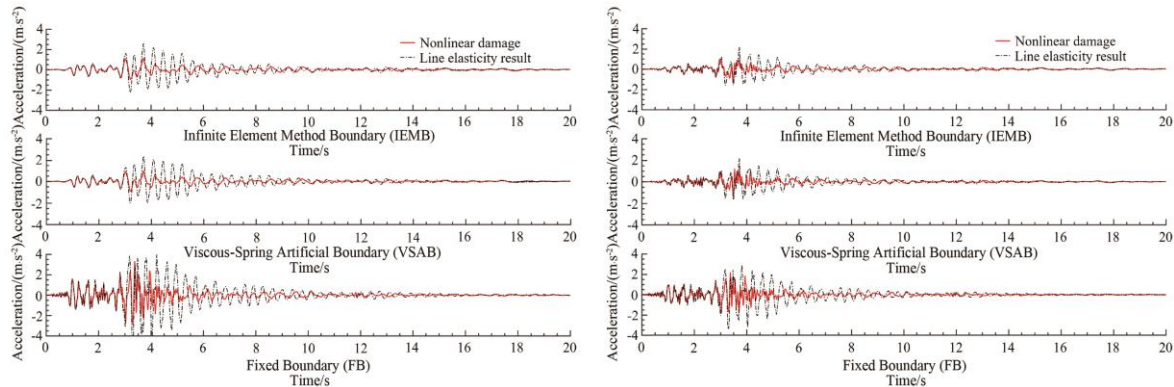


*(a) Lateral flow acceleration at bent (point a); (b) Lateral flow acceleration at crossbeam (point b)*
*Fig. 8 – Contrast diagram of each feature point's acceleration time histories*

*Note: *Feature point positions are shown in Figure 5(b).*

As can be seen from the acceleration time histories of the aqueduct structure shown in Figure 8, the acceleration development trend of each feature point is basically the same under three different boundary conditions, and the maximum response occurs at a time of about 3 s, which is basically consistent with the occurrence time of the seismic peak acceleration. When considering plastic damage during strong earthquakes, the material will occur damage accumulation effect. The change rule of structural acceleration has a strong fluctuation, and the peak value is slightly lower than that in the undamaged state. With the increase in the height of the structure, the acceleration response tends to be amplified, and the displacement of the crossbeam at a lower position is less than that of the bent with a higher position. Finally, by comparing the calculation results of the IEMB and the VSAB, it is found that the difference between the two results is very small, ranging from 0.4% to 19%, but generally below 10%. The FB is 27%–77% larger than the IEMB and 38%–76% higher than the VSAB.

***Aqueduct structure displacement response rules***

The displacement change rule of each feature point of the aqueduct relative to the foundation is shown in Figure 9. During strong earthquakes, the displacement response of each feature point reaches its maximum value at times up to about 4 s, which is the same as the time when the seismic peak ground acceleration occurs. Before the duration of about 3 s, the earthquake excitation is small. During this time, the structure is in the elastic stage, so there was little difference in the response results whether to consider the damage. However, in the late period of the seismic duration, the structural displacement response has a certain displacement deviation from the foundation. The structure undergoes irreversible plastic damages during the earthquake. This is mainly due to the introduction of the CDP constitutive, which can describe the softening behaviour of a concrete structure after damage. The difference between the calculation results of the IEMB and the VSAB is between 2% and 17%. The difference is caused by the difference in the realization of IEMB and VSAB and the processing method of energy dissipation. The results show that the FB increases by 9%–35% compared with the IEMB, and increases by 6%–48% compared with the VSAB.

-------------------------------------------------------------------------------------------------------
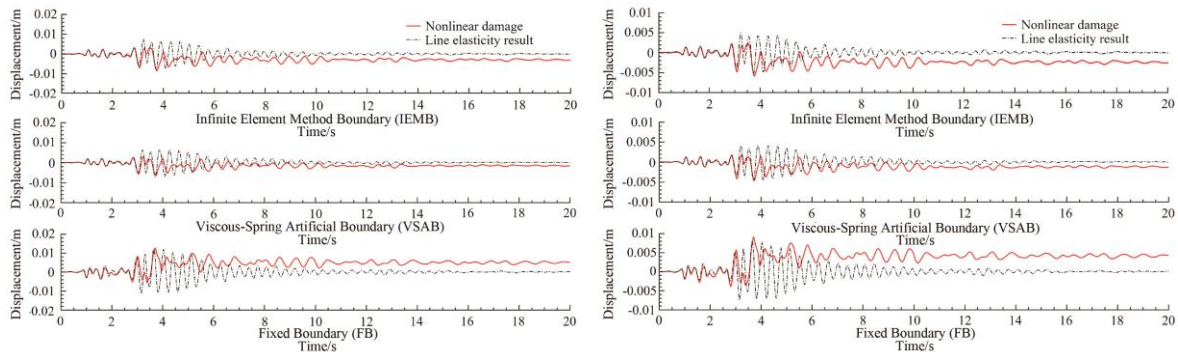


*(a) Lateral flow displacement at bent (point a); (b) Lateral flow displacement at crossbeam (point b)*
*Fig. 9 – Contrast diagram of each feature point's displacement time histories*

*Note: *Feature point positions are shown in Figure 5(b).*

## Dynamic failure mechanism and the damage development rules of the aqueduct structures

Figure 10 reveals the dynamic damage development process of the aqueduct structure. During a strong earthquake, the damage to the bent column is relatively serious. Penetrating damage occurred at the top and bottom of the bent column and both ends of the crossbeam, but no damage occurred at the foundation cushion cap; due to the rigidity of the aqueduct structure, only slight damage was found only near the support of the bent. During the process of damage development, the structural damage to the aqueduct first appeared at the bottom of the bent column and the contact part of foundation at a time of 1.4 s, then the damage occurred at the top of bent in 1.48 s. From 1.48 s–2.82 s, the damage expanded from the bottom of the bent column to the upper part, and damage starts at the end of the lower crossbeam at 2.82 s, as shown in Figure 10(a) and Figure 10(b). Then, from 2.82 s–3.01 s, the damage to the lower crossbeam gradually spreads, and damage begins to appear at the upper crossbeam at a time of 3.01 s. A damage diagram is presented in Figures 10(b) and 10(c). During the seismic duration from 3.01 s–4.01 s, the damage is extended from the top and bottom of the bent to the crossbeam in the middle of the bent. The penetrating damage occurs at the top and bottom of the bent column and the crossbeam, respectively, as shown in Figure 10(d). Finally, in the last part of the seismic duration, the structural damage basically does not change because the seismic acceleration decreases.
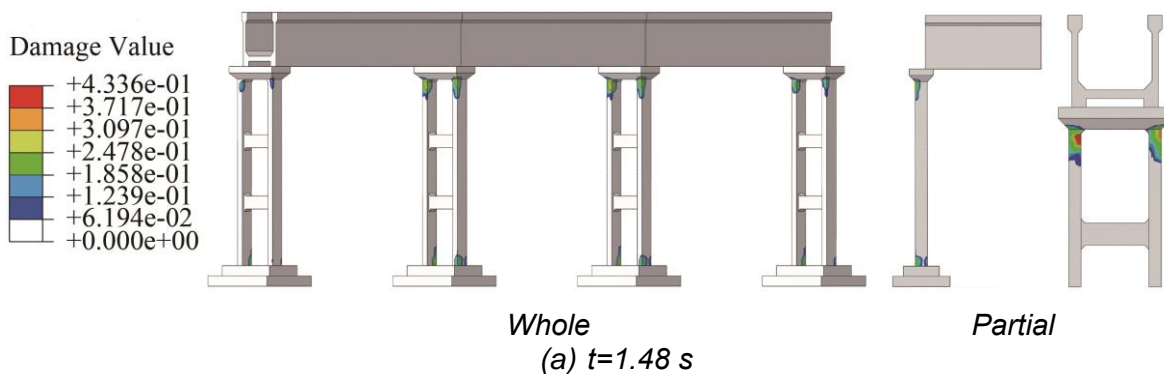


*Whole*                    *Partial*
*(a) t=1.48 s*
*Fig. 10 – Developing process of aqueduct's damage under earthquake*

-----------------------------------------------------------------------------------------------------



*Whole*            *Partial*
*(b) t=2.82 s*

*Whole*            *Partial*
*(c) t=3.01 s*

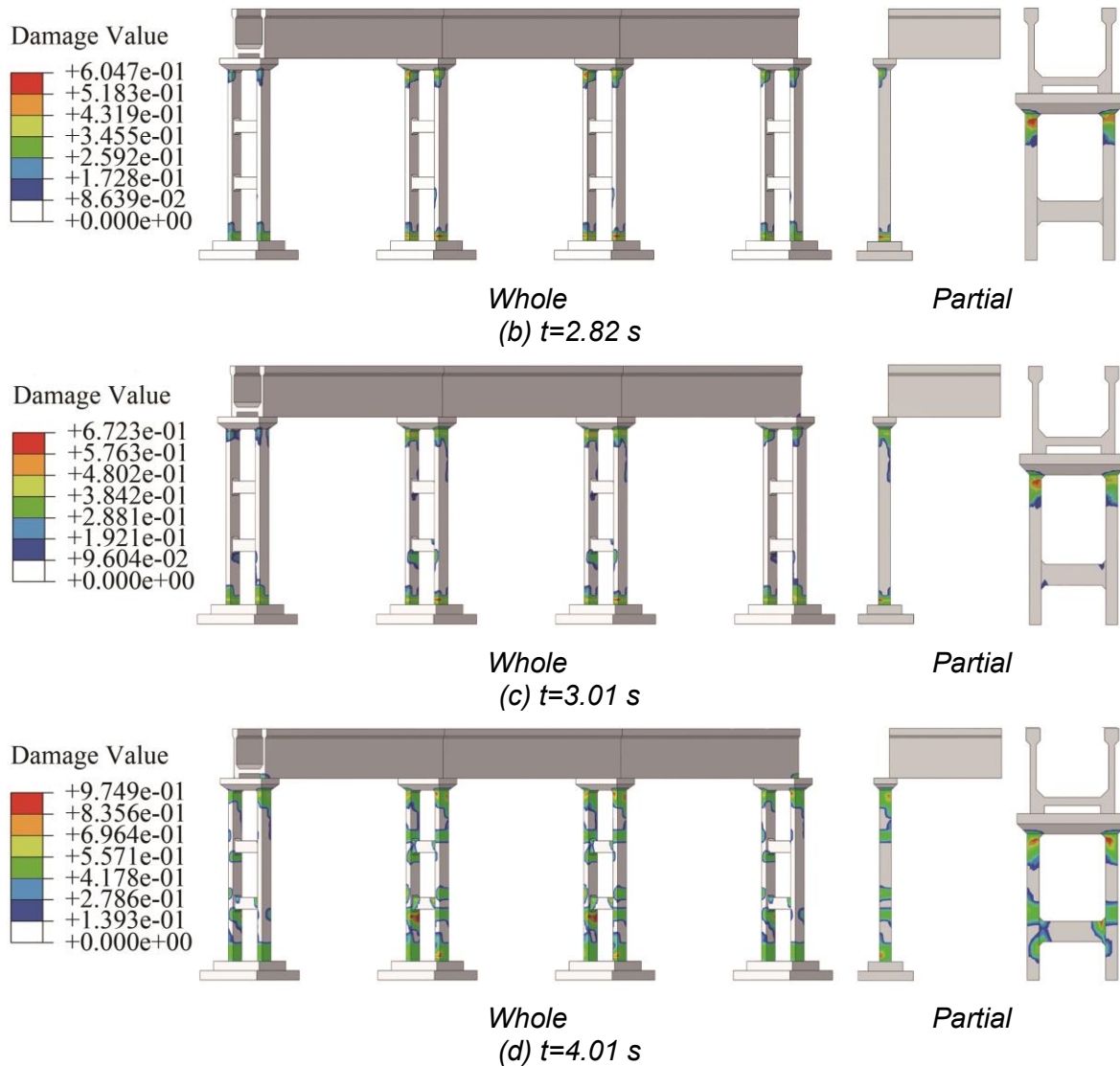*Whole*            *Partial*
*(d) t=4.01 s*
*Fig. 10 – Developing process of aqueduct's damage under earthquake*

The seismic action is closely related to the duration, During seismic wave motion, changes in the acceleration will also cause the structural stress state to change, which is a significant feature of dynamic load time history calculation. To order to explore the development process and rules of aqueduct structural damage during seismic wave motion, the feature points on one side of the structure are selected for analysis. The location of the feature points is shown in Figure 5(a), and the development and changes of damage value at each point are shown in Figure 11. The damage develops extremely rapidly during the course of the earthquake, and is complete in less than 4 s. After the top and bottom of the bent column are damaged, the damage extends to the middle of the bent column; therefore, the time at which damage occurs at the two crossbeams is the same, and soon reaches the complete damage. Compared with the time at which damage occurred at the bent and crossbeams, damage occurred at the bottom of the wing wall near the cushion cap at a relatively late time. After certain damage, the damage no longer changes.
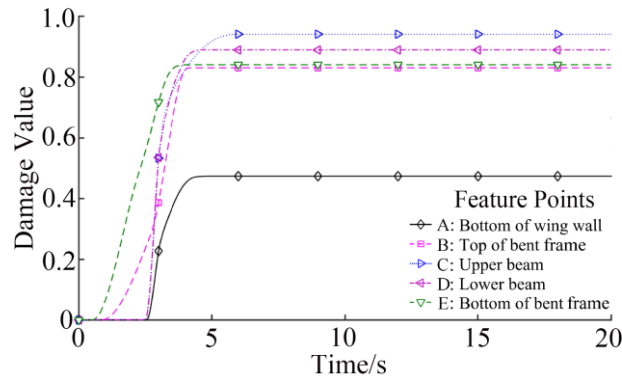
-------------------------------------------------------------------------------------------------------



*Fig. 11 - Feature point damage development process*

*Note: *Feature point positions are shown in Figure 5(a).*

When the seismic ground motion acceleration reaches its peak value, the damage to the structure increases rapidly, indicating that the seismic peak ground motion acceleration has a significant impact on the damage of the structure. When comparing the development trend of damage at each position, it can be seen that the higher the position, the faster the damage development. At the bottom of the bent, the rate of damage development obviously lags behind that of other sections of the structure. A preliminary conclusion is that a higher the position causes a greater displacement and the faster the damage development. The above analysis reflects that the aqueduct structure is most likely to be seriously damaged at the junction of the pier cap and bent column during an earthquake, followed by the two ends of the crossbeam. Once the damage and cracking are serious, the whole aqueduct structure may collapse.

## CONCLUSIONS

In this study, the IEMB, VSAB, FB methods and the CDP constitutive are adopted to study the mechanism and development rules of damage to large–scale irrigation aqueducts under the ground motion of an earthquake. The main conclusions are as follows:

(1)     The effects of conventional FB, VSAB, and dynamic IEMB on the energy absorption and dissipation of impulse waves are compared. The FB cannot absorb the wave energy, and the displacement response will be enlarged by 6%–48% compared with the other two boundaries. Both the VSAB and the dynamic IEMB have a good energy absorption effect on the incident wave, with an error value between 2% and 17%. In the calculations for the towering cantilever structure model, the energy absorption of IEMB is slightly better than that of VSAB. Compared with VSAB, dynamic IEMB does not need a spring–damper mechanical system, and is simpler in form and more efficient in exact modelling.

(2)     In aqueduct seismic ground motion response studies, it was found that with an increase in the height of the structure, the dynamic displacement response of aqueduct trends to enlarge. At the end of the seismic ground motion duration, large–scale damage occurred to the aqueduct support frame, resulting in a slight deviation from the structure displacement relative to the foundation.

(3)     Through the analysis of the damage development rule, it discoveries that the failure position of aqueduct structure is mainly focused on the intersection place of pier cap and bent column, and the intersection place of the bent column and the foundation of an aqueduct. It can be seen that the damage at the bottom of the pier cap appears a general down–slope tendency. These places are in weak areas of the aqueduct structure. Therefore, in the process of seismic design, relevant damping measures should be taken to control the damage development and prevent the overall aqueduct structure from being damaged or collapsed.

-------------------------------------------------------------------------------------------------------

## ACKNOWLEDGEMENTS

## REFERENCES

[1]     Housner G.W., 1963. The dynamic behavior of water tanks, Bulletin of the seismological society of America, vol. 53, no. 2. pp. 381-387.

[2]     Olson L.G., and Bathe K.-J., 1985. Analysis of fluid-structure interactions. A direct symmetric coupled formulation based on the fluid velocity potential, Computers & Structures, vol. 21, no. 1-2. pp. 21-32.

[3]     Omidinasab F., and Shakib H., 2012. Seismic response evaluation of the RC elevated water tank with fluid-structure interaction and earthquake ensemble, KSCE Journal of Civil Engineering, vol. 16, no. 3. pp. 366-376.

[4]     Ibrahim R.A., 2005, Liquid sloshing dynamics: theory and applications (Cambridge University Press).

[5]     Liu Y., Dang K., and Dong J., 2017. Finite element analysis of the aseismicity of a large aqueduct, Soil Dynamics and Earthquake Engineering, vol. 94. pp. 102-108.

[6]     Zhang H., Sun H., Liu L., and Dong M., 2013. Resonance mechanism of wind-induced isolated aqueduct–water coupling system, Engineering structures, vol. 57. pp. 73-86.

[7]     Ying L., Meng X., Zhou D., Xu X., Zhang J., and Li X., 2019. Sloshing of fluid in a baffled rectangular aqueduct considering soil-structure interaction, Soil Dynamics and Earthquake Engineering, vol. 122. pp. 132-147.

[8]     Li Y., Lou M., and Pan D., 2003. Evaluation of vertical seismic response for a large‐scale beam‐supported aqueduct, Earthquake engineering & structural dynamics, vol. 32, no. 1. pp. 1-14.

[9]     Zarghamee M.S., Rao R.S., Kan F.W., Keller T.O., Yako M.A., and Iglesia G.R., 1997. Seismic risk analysis of hultmann aqueduct, Infrastructure Condition Assessment: Art, Science, and Practice. pp. 346-355.

[10]    Chrysostomou C.Z., Stassis A., Demetriourder T., and Hamdaoui K., 2008. Application of shape memory alloy prestressing devices on an ancient aqueduct, Smart Structures and Systems, vol. 4, no. 2. pp. 261-278.

[11]    Lysmer J., and Kuhlemeyer R.L., 1969. Finite dynamic model for infinite media, Journal of the Engineering Mechanics Division, vol. 95, no. 4. pp. 859-878.

[12]    Deeks A.J., and Randolph M.F., 1994. Axisymmetric time-domain transmitting boundaries, Journal of Engineering Mechanics, vol. 120, no. 1. pp. 25-42.

[13]    Gu Y., Liu J.B., and Du Y., 2007. 3D consistent viscous-spring artificial boundary and viscous-spring boundary element, Engineering Mechanics, vol. 24, no. 12. pp. 31-37.(in Chinese)

[14]    Liao Z.P., and Wong H., 1984. A transmitting boundary for the numerical simulation of elastic wave propagation, International Journal of Soil Dynamics and Earthquake Engineering, vol. 3, no. 4. pp. 174-183.

[15]    Ungless R.F., 1973. Infinite finite element.

[16]    Bettess P., 1984. A new mapped infinite element for exterior wave problems, Numerical methods in coupled systems.

[17]    Zienkiewicz O., Bando K., Bettess P., Emson C., and Chiam T., 1985. Mapped infinite elements for exterior wave problems, International Journal for Numerical Methods in Engineering, vol. 21, no. 7. pp. 1229-1251.

[18]    Yun C.B., Kim D.K., and Kim J.M., 2000. Analytical frequency-dependent infinite elements for soil–structure interaction analysis in two-dimensional medium, Engineering structures, vol. 22, no. 3. pp. 258-271.

[19]    Qi Y., and Hisanori O., 2014. Study of ABAQUS dynamic infinite element artificial boundary, Rock and Soil Mechanics, vol. 35, no. 10. pp. 3007-3013.(in Chinese)

[20]    Zhang C.H., and Zhao C. B., 1987. Coupling method of finite and infinite elements for strip foundation wave problems, Earthquake engineering & structural dynamics, vol. 15, no. 7. pp. 839-851.

[21]    Godbole P.N., Viladkar M.N., and Noorzaei J., 1990. Nonlinear soil-structure interaction

analysis using coupled finite-infinite elements, Computers & Structures, vol. 36, no. 6. pp. 1089-1096.

[22]      Viladkar M.N., Godbole P.N., and Noorzaei J., 1991. Soil-structure interaction in plane frames using coupled finite-infinite elements, Computers & Structures, vol. 39, no. 5. pp. 535-546.

[23]      Edip K., Garevski M., Butenweg C., Sesov V., Cvetanovska J., and Gjorgiev I., 2013. Numerical simulation of geotechnical problems by coupled finite and infinite elements, Journal of Civil Engineering and Architecture, vol. 7, no. 1. p. 68.

[24]      Xu X.Y., Ma Z.Y., and Zhang H., 2013. Simulation algorithm for spiral case structure in hydropower station, Water Science and Engineering, vol. 6, no. 2. pp. 230-240.

[25]      Lee J., and Fenves G.L., 1998. Plastic-damage model for cyclic loading of concrete structures, Journal of Engineering Mechanics, vol. 124, no. 8. pp. 892-900.

[26]      Oliver J., Oller S., and Oñate E., 1989. A plastic-damage model for concrete, International Journal of solids and structures, vol. 25, no. 3. pp. 299-326.

[27]      He J.T., Ma H.F., Zhang B.Y., and Chen H.Q., 2010. Method and realization of seismic motion input of viscous-spring boundary, Shuili Xuebao(Journal of Hydraulic Engineering), vol. 41, no. 8. pp. 960-969.

[28]      Lamb H., 1903. On the Propagation of Tremors over the Surface of an Elastic Solid, Proceedings of the royal society of London, vol. 72. pp. 128-130.

[29]      Kanai K., 1983, Engineering seismology (University of Tokyo Press).